January 1992

The effect of diamagnetic dilution on the spin-phonon interaction and scattering cross section in Fe1-xZnxF2

Christian Binek
University of Nebraska-Lincoln, cbinek@unl.edu

J. Phys.: Condens. Matter 4 (1992) 65–74. Printed in the UK

The effect of diamagnetic dilution on the spin–phonon interaction and phonon scattering cross section in $Fe_{1-x}Zn_xF_2$

C Binek and W Kleemann
Angewandte Physik, Universität Duisburg, W-4100 Duisburg 1, Federal Republic of Germany

Received 3 April 1991, in final form 27 August 1991

Abstract. The temperature dependences of the first moments of phonon Raman scattering lines are studied for $Fe_{1-x}Zn_xF_2$. The diamagnetic dilution diminishes the spin–phonon coupling strength of phonons with both A_{1g} and E_g symmetry in proportion to the decrease in the ordering temperature T_N. Moreover, the E_g mode shows an asymmetrical lineshape for Zn concentrations $x > 0.3$. It is explained by an unresolved superposition of two modes, one of which is ascribed to perturbed ZnF_2 with broken translational symmetry.

1. Introduction

Perturbations of Raman light scattering spectra in solids due to structural disorder on the one hand [1] and to magnetic interactions on the other hand [2] have been of major interest in the past few decades. More recently, the simultaneous consideration of both structural and magnetic disorder has become a particularly challenging subject to Raman spectroscopists. Within this context, most work on disordered magnets has been devoted to the exploration of their various magnetic excitations [3]. Relatively little attention, however, has been given to the peculiar behaviour of the optical phonons in these systems. They are known to probe both structural disorder [1] and magnetic interactions via spin–phonon coupling [2]. Special emphasis was put on verifying the predicted [1] linear concentration dependence of the Raman line positions in mixed antiferromagnets such as $Mn_{1-x}Zn_xF_2$ [4], $Fe_{1-x}Mn_xCl_2$ [5], $Fe_{1-x}Co_xCl_2$ [6] and $Fe_{1-x}Zn_xF_2$ [7]. More sophisticated effects such as line broadening due to concentrational fluctuations and two-mode behaviour [1], occasionally observed on selected optical phonon lines, were discussed in a rather preliminary fashion only [7]. No attempt at all has been made to investigate the temperature dependence of the line positions in disordered magnets. As is well known from the study of pure systems such as FeF_2 [8] the low-temperature line shift is expected to be proportional to the thermal variation in the spin–spin correlation function [2]. Characteristic deviations from the behaviour found in pure systems are expected in particular in the vicinity of the ordering temperature. The relevance of disorder to the critical behaviour of spin correlations has been verified by various other investigations including optical techniques such as linear birefringence [9] or exciton magnon absorption [10].

0953-8984/92/010065 + 10 $03.50

This paper is aimed at a detailed Raman investigation of the optical phonons in the diluted Ising antiferromagnet $Fe_{1-x}Zn_xF_2$, thus continuing previous work [7] in the spirit of now-classical investigations on the pure system [8]. We studied the temperature dependences of the first moments of the A_{1g} and E_g phonon scattering lines for concentrations $x = 0$, 0.4 and 0.53. Theoretical considerations, based on early work on ferromagnets [11], are extended to explain the influence of the magnetic dilution on both the spin–spin correlation function $\langle S_0 \cdot S_1 \rangle$ and the spin-phonon coupling coefficient λ. We observe a proportionality of λ with the Néel temperature $T_N(x)$, which is explained in terms of a novel mean-field-type calculation.

Furthermore, we focus our attention again [7] on the peculiar concentration dependence of the E_g phonon scattering lineshape. It might be considered as an interesting test for the criteria to classify the phonons in disordered systems according to the occcurrence of either one- or two-mode behaviour [1]. In the low-dilution limit these criteria have usually [1] been traced back to the existence of either local or gap or extended phonon states. At intermediate concentrations, more sophisticated considerations have to be adopted in order to obtain reasonable predictions [12]. In this paper we present a new attempt to understand qualitatively the shape of the E_g mode scattering line in the entire concentration range $0 < x < 1$ consistent with our own and previous [7] results.

2. Experimental details

The Raman spectra were excited by filtered argon laser light at 488 nm. Owing to non-negligible absorption [10] the power was kept as low as approximately 100 mW in order to avoid sample heating. The scattered light intensity was measured in $x(yy)z$ and $x(zy)z$ polarizations in order to select A_{1g} and E_g phonon lines, respectively. x, y and z are chosen to lie along the crystal axes a, b and c. The scattered light was collected with an $f/1.2$ camera lens dispersed by an ISA–Jobin–Yvon U 1000 double monochromator at a spectral resolution of 0.92 cm^{-1} and detected with a cooled Hamamatsu R943-02 photomultiplier tube. Samples with typical edge lengths of 2–3 mm of FeF_2, $Fe_{0.6}Zn_{0.4}F_2$ and $Fe_{0.47}Zn_{0.53}F_2$ were cut and polished parallel to the {100} faces of Bridgman-grown single crystals (grown by N Nighman, Physics Department, University of California, Santa Barbara). The samples were mounted in the exchange gas of a helium-evaporation-type cryostat. Temperatures between $T = 4.2$ and 300 K could be stabilized to better than 0.1 K. Measurements of the principal linear birefringence Δn_{ac} were performed at $\lambda = 589.3$ nm using standard techniques [13] in order to determine independently the temperature dependence of the spin–spin correlation function.

3. Experimental results

Figure 1(a) and 1(b) show two low temperature Raman spectra of phonon modes with A_{1g} and E_g symmetries, respectively, obtained for $Fe_{0.47}Zn_{0.53}F_2$ at $T = 11.3$ K and $T = 33.9$ K, respectively. Whereas the A_{1g} line looks essentially symmetric, the E_g phonon has a non-Lorentzian lineshape, which will be discussed below. Figures 2(a) and 2(b) show the temperature dependences of the first moments of Raman scattering lines of the A_{1g} and E_g modes, respectively, for $Fe_{0.6}Zn_{0.4}F_2$. The full curves represent the temperature dependences in the absence of spin–phonon coupling as expected from

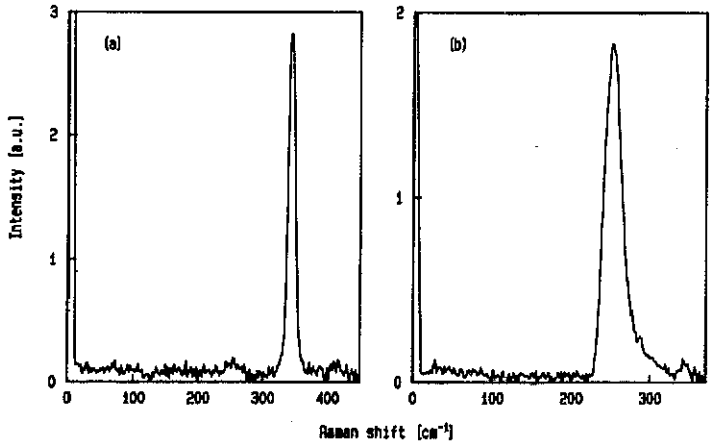

Figure 1. Raman spectrum of (*a*) the A_{1g} and (*b*) the E_g phonons obtained for $Fe_{0.47}Zn_{0.53}F_2$ at $T = 11.3$ K and 33.9 K, respectively.

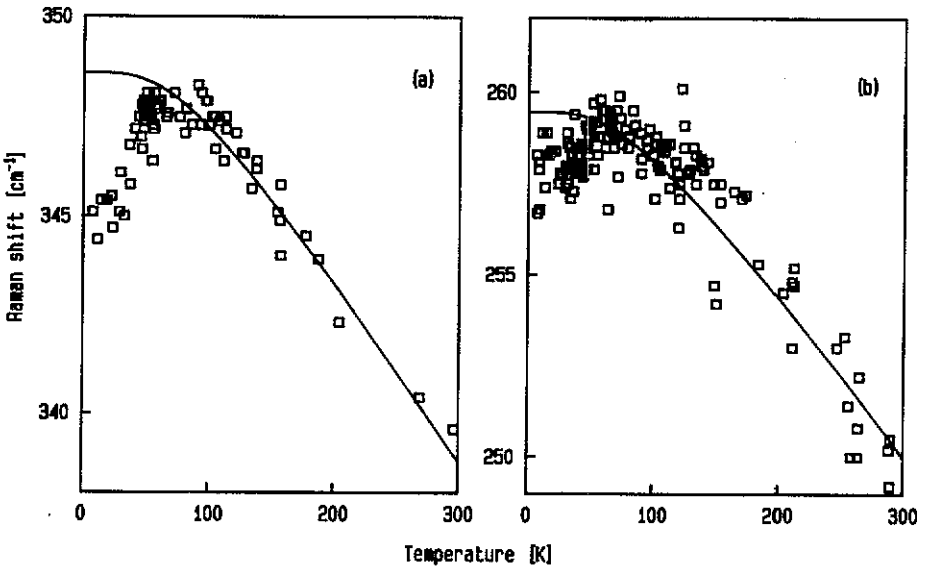

Figure 2. Temperature dependences of the first moments of the Raman scattering lines of (*a*) the A_{1g} and (*b*) the E_g phonons measured in $Fe_{0.6}Zn_{0.4}F_2$ (□) and theoretically expected from best-fitted Debye-type energy functions in the absence of spin–phonon coupling (——).

best fits to Debye-type energy functions in the high-temperature range ($T > 2T_N$; see discussion below). Magnetic anomalies are clearly observed in the low-T range ($T \leqslant 50$ K), yielding total low energy shifts of the order of 2–4 cm^{-1} as $T \rightarrow 0$. Similarly, both phonons were investigated on samples with $x = 0$ and 0.53. The results are compared in the following section.

4. Theory and comparison with experimental results

4.1. Spin–phonon coupling in diluted antiferromagnets

In complete analogy to the considerations applied to ferromagnets in [11] we obtain the total magnetic frequency shift $\Delta\omega$ relative to the phonon frequency ω_0:

$$\frac{\Delta\omega}{\omega_0} = \left(\kappa\gamma\frac{\partial}{\partial\Omega}\sum_{\langle ij\rangle}J_{ij} + \frac{1}{2\omega_0^2}\sum_{\langle ij\rangle}\frac{\partial^2 J_{ij}}{\partial u^2}\right)\langle S_0 \cdot S_1\rangle \tag{1}$$

with the isothermal compressibility κ and the Grüneisen parameter γ connecting the relative change in the volume Ω with a relative frequency shift. $\langle ij\rangle$ denotes a summation over all pairs of nearest-neighbour sublattice positions i, j which are occupied by cations. We assume J_{ij} to be be normalized to the total number of summations and only non-vanishing if both positions i and j are occupied by Fe^{2+} ions. Since extensive spin quantities of macroscopic samples do not depend on a special spin configuration, we are allowed to deduce equation (1) either from a special or from the impurity-averaged free energy. Hence, $\langle S_0 \cdot S_1\rangle$ may be called a generalized average of the spin product, which means thermal as well as impurity average. In contrast with the treatment in [11] the derivatives of the superexchange constants J_{ij} have not explicitly been calculated using symmetry-adapted ion displacements and the specific crystal structure. Here the derivatives have a more symbolic character, indicating the implicit dependence of the J_{ij} on the volume and normal coordinate u. According to [8] we introduce the spin–phonon coupling coefficient

$$\lambda = \kappa\gamma\omega_0(\partial J/\partial\Omega) + (2\omega_0)^{-1}(\partial^2 J/\partial u^2) \tag{2}$$

where $J = \Sigma_{\langle ij\rangle} J_{ij}$.

The diamagnetic dilution has two effects on the magnetic part of the Raman frequency shift. On the one hand, the thermal decay of $\langle S_0 \cdot S_1\rangle$ is correlated with the gradual decrease in T_N as x increases. As long as $1 - x$ exceeds the percolation threshold, however, the low-T limit $\langle S_0 \cdot S_1\rangle(T = 0) = -S^2$ is universal for all x. On the other hand the coupling coefficient λ depends on x as well. This effect is readily obtained from $\Delta\omega$ in the limit $T \to 0$. Equation (2) contains all quantities which might be influenced by dilution. The concentration dependence of J is due to the statistical replacement of Fe^{2+} by Zn^{2+} ions such that some J_{ij} vanish, whereas κ, γ and Ω have only a weak concentration dependence as a consequence of comparable material parameters of FeF_2 and ZnF_2 [14]. However, the phonon frequencies ω_0 differ perceptibly when alloying FeF_2 with ZnF_2 [7]. Therefore one has

$$d\lambda/dx = (\partial\lambda/\partial\omega_0)(\partial\omega_0/\partial x) + (\partial\lambda/\partial J)(\partial J/\partial x). \tag{3}$$

The partial derivatives of λ entering this expression are obtained by inspection of (2). Firstly, we obtain

$$\partial\lambda/\partial\omega_0 = \kappa\gamma(\partial J/\partial\Omega) - (2\omega_0^2)^{-1}(\partial^2 J/\partial u^2). \tag{4}$$

Secondly, in order to calculate $\partial\lambda/\partial J$ approximately, we introduce a single lattice constant a as a cubic approximation of the tetragonal structure. It enters an expression for the superexchange constant, $J = J_0 \exp(-r/a)$, where J_0 contains the concentration

Table 1. Absolute and relative Néel temperatures, $T_N(x)$ and $T_N(x)/T_N(0)$, respectively, magnetic phonon frequency shifts $\Delta\omega$ and absolute and relative spin–phonon coupling constants, $\lambda(x)$ and $\lambda(x)/\lambda(0)$, respectively, determined for the A_{1g} and the E_g Raman modes in $Fe_{1-x}Zn_xF_2$ with $x = 0$, 0.4 and 0.53.

			$\Delta\omega(T=0\,K)$ (cm^{-1})		$\lambda(x)$ (cm^{-1})		$\lambda(x)/\lambda(0)$	
x	$T_N(x)$	$T_N(x)/T_N(0)$	A_{1g}	E_g	A_{1g}	E_g	A_{1g}	E_g
0	78.4	1	5.94	2.17	1.49	0.54	1	1
0.4	47.1	0.60	3.87	1.53	0.97	0.38	0.6	0.71
0.53	36.4	0.46	3.41	1.15	0.85	0.29	0.5	0.53

dependence of J and r is the typical length of the superexchange path. By taking into account that $r = r(u)$ one readily obtains the expression

$$\partial^2 J/\partial u^2 = [-(1/a)(\partial^2 r/\partial u^2) + (1/a^2)(\partial r/\partial u)^2]J. \tag{5}$$

Furthermore, in the cubic approximation $\Omega = a^3$, we obtain

$$\partial J/\partial \Omega = (r/3a^4)J. \tag{6}$$

Insertion of this and equation (5) into equation (2) yields

$$\partial\lambda/\partial J = \kappa\gamma\omega_0 r/3a^4 + (1/2\omega_0)[-(1/a)(\partial^2 r/\partial u^2) + (1/a^2)(\partial r/\partial u)^2]. \tag{7}$$

Application of Vegard's rule to both ω_0 and J yields $\partial\omega_0/\partial x \simeq \omega_0(x=1) - \omega_0(x=0) = \Delta\omega_0$ and $\partial J/\partial x \simeq J(x=1) - J(x=0) = -J(x=0)$. Inserting these approximations into (3) together with (4) and (7) we finally obtain

$$\begin{aligned}\partial\lambda/\partial x = {} & \{\kappa\gamma r/3a^4 - (1/2\omega_0^2)[-(1/a)(\partial^2 r/\partial u^2) + (1/a^2)(\partial r/\partial u)^2]\}J(x)\,\Delta\omega_0 \\ & + \{-\kappa\gamma r/3a^4 - (1/2\omega_0^2)[-(1/a)(\partial^2 r/\partial u^2) + (1/a^2)(\partial r/\partial u)^2]\}J(x=0)\omega_0.\end{aligned} \tag{8}$$

Taking into account that $|J(x=0)| > |J(x)|$ and $\omega_0 \gg |\Delta\omega_0|$ at all concentrations $0 < x < 1$, we see that only the second term of (8) is important. Therefore equation (3) simplifies to $d\lambda/dx \simeq (\partial\lambda/\partial J)(\partial J/\partial x)$. Since we are allowed to neglect the concentration dependence of ω_0 in equation (2) we obtain $\partial\lambda/\partial J \simeq d\lambda/dJ$. Inserting (5) and (6) into equation (2) and comparing this with equation (7) we readily see that $d\lambda/dJ = \lambda/J$. With the usual arguments of mean-field theory [15] we connect $J(x)$ with the concentration-dependent transition temperature $T_N(x)$ and obtain by integration

$$\lambda(x)/\lambda(0) = T_N(x)/T_N(0). \tag{9}$$

Comparison with our experimental results is shown in table 1. The magnetic Raman shifts $\Delta\omega(T=0)$ are listed for $x = 0$, 0.4 and 0.53. They are transformed into $\lambda(x)$ via equations (1) and (2) with $\langle S_0 \cdot S_1\rangle(T=0) = -4$, since $S = 2$ for Fe^{2+} in $Fe_{1-x}Zn_xF_2$. As indicated in figure 2, $\Delta\omega(T=0)$ is obtained by subtracting the lattice contribution to ω versus T. Using the assumption that all lattice modes obey a unique Grüneisen law we find that the frequency shift due to thermal expansion is proportional to the thermal lattice energy [16]. A Debye model approximation with fixed Debye temperature Θ_D =

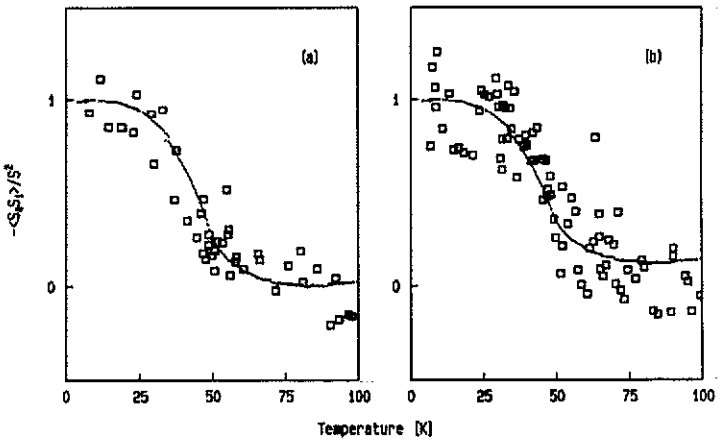

Figure 3. Magnetic contribution to the total Raman frequency shift (□) of (*a*) the A_{1g} and (*b*) the E_g phonons and the linear magnetic birefringence (· · · ·) in $Fe_{0.6}Zn_{0.4}F_2$ as a function temperature, both normalized to their maximum value.

300 K, interpolating between various values found in the literature [17, 18], was used to fit the data at $T > 2T_N$. The coupling coefficients of the pure FeF_2 agree satisfactorily with previous results [8] despite the fact that they are obtained by different methods of evaluation. Reasonable agreement between $\lambda(x)/\lambda(0)$ and $T_N(x)/T_N(0)$ as expected from equation (9) is found within an error of about 10%.

Finally, we compare the light scattering results with a measurement of the linear magnetic birefringence, which is known to be an accurate measure of the spin-pair correlation function [9]. Figure 3 shows the magnetic Raman frequency shifts (open squares) of the A_{1g} and E_g phonons and the linear magnetic birefringence (dotted curves) for $Fe_{0.6}Zn_{0.4}F_2$, both normalized to their maximum value. In the case of the strongly scattering E_g-phonon data the proportionality with the birefringence curve is most convincingly shown by a least-squares fit of both sets of data allowing for a slight residual birefringence as $T \rightarrow 100$ K. This seems to indicate a slight positive shift of the Raman data baseline compared with that which was determined from a Debye-type background at high temperatures. Despite the considerable scatter of the light scattering data both methods yield clearly compatible results. This holds, too, for the sample with $x = 0.53$, whose birefringence data were taken from [9]. The good agreement confirms the validity of our background subtraction procedure from the total Raman shift, ω versus T.

4.2. Phonon scattering cross section for Zn concentrations $x > 0.3$

It is known [7] that the E_g-phonon scattering line of $Fe_{1-x}Zn_xF_2$ shows a typical two-mode behaviour [1] in the low-concentration range $x < 0.3$. It can be described by two independent superimposed Lorentzian lines characterizing the FeF_2- and the ZnF_2-like mode. This concept is definitely not applicable to systems with higher concentrations. As shown in figure 4(*a*) for the E_g-phonon line in $Fe_{0.47}Zn_{0.53}F_2$ (digitized presentation of an E_g-phonon line measured at $T = 33.9$ K shown by open circles), a best two-Lorentzian fit (full curve) does not model the steep increase in the intensity at low frequencies. Similar observations hold for larger Zn^{2+} concentrations, e.g. when replacing $x = 0.53$ by $x = 0.9$ (figure 4(*b*)); digitized experimental data [7] shown by open

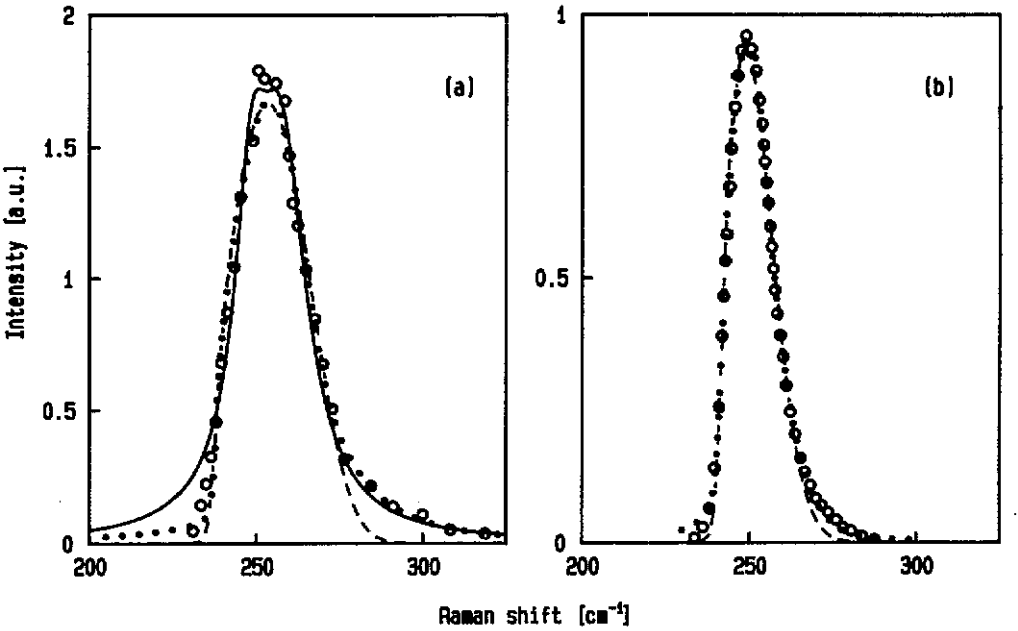

Figure 4. Digitized representations of the E_g phonon lines (○) measured (*a*) at $T = 33.9$ K for $Fe_{0.47}Zn_{0.53}F_2$ and (*b*) at $T = 20$ K for $Fe_{0.1}Zn_{0.9}F_2$ (data taken from [7]), best two-Lorentzian fit (——), best fits by use of the ZnF_2-like mode $Z_1(\omega)$ (– – –) and best fit of the total lineshape function $Z(\omega)$ (· · ·) involving $Z_1(\omega)$ and the FeF_2-like mode $Z_2(\omega)$ (see text).

circles). Hence, the steep low-frequency shoulder is obviously characteristic of large Zn concentrations.

The lineshape is strongly reminescent of that found in heavily doped p-type silicon [19], the phonon excitation of which exhibits a Fano-type interference with continuously distributed low-energy electronic states [20]. Such a possibility cannot be ruled out *a priori* for $Fe_{1-x}Zn_xF_2$, since low-energy electronic excitations are, indeed, present because of spin–orbit splitting of the $^5T_{2g}$ ground state of Fe^{2+}. The Γ_{3g} and Γ_{4g} excitons lie at an energy of about 154 cm^{-1} above the Γ_{5g} ground state in FeF_2 [21]. However, this energy is sharp throughout the flat exciton band and very probably does not vary significantly when changing the Zn^{2+} concentration [10]. Hence, interference and anti-resonance with the E_g-phonon state, which lies between 250 and 270 cm^{-1} in the $Fe_{1-x}Zn_xF_2$ system for all x [7], can rather safely be excluded.

The difference between of the lineshapes in the two concentration limits $x \rightarrow 0$ and $x \rightarrow 1$ is explained as follows. On the one hand, low Zn concentrations are assumed to change the force constants such that local modes split off from band modes of the pure FeF_2 system and lead to the observed two-mode behaviour. It should be mentioned that the usual mass criterion used within this context [1] fails, because only the F^--ion positions enter the displacement vector of the Raman-active phonons [22], whereas the Fe^{2+} and Zn^{2+} ions occupy invariable equilibrium positions.

On the other hand, low Fe^{2+} concentrations in a matrix of ZnF_2 give rise to extended phonon states, whose energies fall within the phonon band of pure ZnF_2. In order to understand the scattering lineshape characteristic of disordered ZnF_2, one has to take

into account the breakdown of translational symmetry due to the FeF_2 impurities. Hence the wavevector q is no longer a good quantum number describing a normal mode of vibration. It is rather described by a superposition of unperturbed normal modes with different q-values. As a consequence, in a light scattering experiment the total wavenumber is not conserved. In other words, excitation of phonon modes with $q \neq 0$ will play an increasing role at increasing disorder. For that reason we introduce a lineshape function

$$Z_1(\omega) = \sum_q P(q)\delta[\omega - \omega(q)] \tag{10}$$

which describes the contribution of different phonon modes by a weighting distribution function $P(q)$, where $q = |\boldsymbol{q}|$. We propose the following analytic *ansatz*:

$$P(q) = (\pi\varepsilon)^{-1/2} \exp(-q^\beta/\varepsilon) \qquad \varepsilon, \beta > 0. \tag{11}$$

In the limit $\varepsilon \to 0$ and $\beta = 2$, $P(q)$ becomes Dirac's δ-function, which corresponds to the idealized pure limit, $Z(\omega) = \delta[\omega - \omega(0)]$. In order to calculate $Z_1(\omega)$ we introduce a parabolic dispersion relation

$$\omega(q) = a + bq^2 \qquad a > 0 \quad b > 0 \tag{12}$$

which holds for the related rutile-type system MgF_2 [23] near $q = 0$. Since $P(q)$ decreases rapidly at finite q, the simplified equation (12) represents a satisfying approximation. When expressing, as usual, $Z_1(\omega)$ as an integral over the whole q-space by use of equation (12) we obtain

$$Z_1(\omega) = (L/2\pi)^3[4\pi/2b(\pi\varepsilon)^{1/2}][(\omega - a)/b]^{1/2} \exp\{-[(\omega - a)/b]^{\beta/2}/\varepsilon\} \qquad \omega > a \tag{13}$$

where L is the linear sample dimension. Clearly $Z_1(\omega) = 0$ for $\omega < a$ because of equation (12). However, in order to describe the smooth onset of the experimentally found intensity shape function (figure 4) due to thermal and instrumental rounding, one has to replace the factor $f_+(\omega) = [(\omega - a)/b]^{1/2}$ in equation (13) by a function $f_-(\omega)$ which rapidly drops to zero as $\omega < a$ and smoothly joins $f_+(\omega)$ at some frequency $\omega_0 \geqslant a$. This condition is fulfilled by the *ansatz*:

$$f_-(\omega) = \{2[(\omega_0 - a)/b]^{1/2} - \tfrac{1}{2}[(\omega_0 - a)/b]^{-1/2}\} \exp(\omega - \omega_0) + \{\tfrac{1}{2}[(\omega_0 - a)/b]^{-1/2} - [(\omega_0 - a)/b]^{1/2}\} \exp[2(\omega - \omega_0)] \tag{14}$$

which contains only one further fitting parameter, ω_0.

Now we are able to describe the contribution of the perturbed ZnF_2 mode to the total lineshape function. The broken curve in figure 4 represent the best fits using equation (13) for $\omega > \omega_0$ and equation (14) for $\omega < \omega_0$, respectively. It is seen that the fit is reasonable for the high Zn concentration $x = 0.9$ (broken curve). However, an appreciable misfit still occurs for $x = 0.53$ on the high-frequency side of the lineshape function. Very probably, this indicates that a contribution due to an FeF_2-like mode is missing in our model calculation.

Hence, in order to obtain the complete lineshape function $Z(\omega)$, which holds in the intermediate concentration range too, we tentatively assume a superposition of two contributions $Z_1(\omega)$ and $Z_2(\omega)$, such that $Z(\omega) = Z_1(\omega) + Z_2(\omega)$. Since we still deal with a modified two-mode concept, it is consequent to involve lineshape functions of both the ZnF_2-like mode ($Z_1(\omega)$; see above) and the FeF_2-like mode ($Z_2(\omega)$) because

of the concentration limits $x \to 1$ and $x \to 0$. As mentioned above, $x \to 0$ creates an independent local ZnF_2 mode which does not influence the Lorentzian character of the dominant FeF_2 mode. We therefore describe $Z_2(\omega)$ by a Lorentz function

$$Z_2(\omega) = \alpha/[(\omega - \omega_2)^2 + \Gamma^2] \tag{15}$$

centred at ω_2 and broadened by virtue of the damping parameter Γ. The resulting total lineshape function $Z(\omega)$ involves nine fitting parameters, which are determined by least-squares routines. The dotted curves in figures 4(*a*) and 4(*b*) show the results of the fitting procedures of the E_g-phonon lines in $Fe_{1-x}Zn_xF_2$ with $x = 0.53$ and $x = 0.9$, respectively. It is seen that the high-energy wings are now satisfactorily modelled.

Some of the fitting parameters can be checked for their physical meanings. Firstly, we check whether the separation of the FeF_2- and ZnF_2-mode peak positions in $Fe_{0.47}Zn_{0.53}F_2$ follows the trend which can directly be observed in the concentration range $x < 0.3$ [7]. The peak position ω_1 of the ZnF_2-like mode given by

$$\omega_1 = a + b(\varepsilon/\beta)^{2/\beta} \tag{16}$$

is easily obtained from equation (13). Inserting the results of the least-squares routines, $a = 236.84\ \text{cm}^{-1}$, $b = 2.44\ \text{cm}^{-1}$ (using q as the dimensionless quantity), $\beta = 8.18$ and $\varepsilon/\beta = 2005.9$, into (16) we obtain $\omega_1 = 252.5\ \text{cm}^{-1}$. The maximum value of $Z_2(\omega)$ is given by the fitting parameter $\omega_2 = 267.6\ \text{cm}^{-1}$. Hence, the separation of the peak positions is $\omega_2 - \omega_1 = \delta\omega = 15.1\ \text{cm}^{-1}$. This result forms an unconstrained continuation of the directly observable separation of the peak positions for $x = 0.12$ ($\delta\omega = 9.7\ \text{cm}^{-1}$) and $x = 0.28$ ($\delta\omega = 13.5\ \text{cm}^{-1}$) reported in [7].

Furthermore we find, very reasonably, a decrease in the Lorentzian mode intensity with increasing Zn concentration. This is already seen by inspection of figures 4(*a*) and 4(*b*) (broken curves) and numerically confirmed by use of the final fitting curves. By integrating the shape function (15), $I_2 = \pi\alpha/\Gamma$, and numerical integration of $Z_1(\omega)$ we find the intensity ratios $I_2/I_1(x = 0.53) = 22/33 = 0.67$ and $I_2/I_1(x = 0.9) = 6/11 = 0.55$, respectively.

5. Conclusion

The concentration dependence of the spin–phonon coupling coefficient in diamagnetically diluted FeF_2 can be explained within the framework of a simple mean-field model. It yields proportionality with the Néel temperature in agreement with the experimental results. The light scattering measurements show a qualitative difference between the A_{1g} and E_g-phonon lineshapes. In contrast with the Lorentzian A_{1g} line the more complex lineshape of the E_g phonon requires a description beyond the virtual-crystal approximation. In the low-x limit, localized impurity modes due to ZnF_2 do not perturb the Lorentzian lineshape function of the dominant FeF_2-like contribution. In contrast with this, in the high-x limit, resonant FeF_2 impurity modes cause a non-negligible change in the lineshape function of the dominant ZnF_2-like mode. In the latter case, for the first time, the breakdown of translational symmetry and, hence, of q conservation has explicitly been taken into account in order to understand the asymmetric lineshape.

Acknowledgments

Thanks are due to Professor V Jaccarino, University of California, Santa Barbara, for providing the excellent samples of the title compounds. Helpful advice with the Raman scattering technique was provided by Th Kleinefeld and D Sommer. This work was in part supported by the Deutsche Forschungsgemeinschaft through Sonderforschungsbereich 166.

References

[1] Chang I F and Mitra S S 1971 *Adv. Phys.* **20** 359
Barker A S and Sievers A J 1975 *Rev. Mod. Phys. Suppl. 2* **47** S1
[2] Cottam M G and Lockwood D J 1986 *Light Scattering in Magnetic Solids* (New York: Wiley)
[3] Cowley R A and Buyers W J L 1972 *Rev. Mod. Phys.* **44** 406
[4] Buchanan M, Buyers W J L, Elliott R J, Harley R T, Hayes W, Perry A M and Saville I D 1972 *J. Phys. C: Solid State Phys.* **5** 2011
[5] Mischler G, Bertrand D, Lockwood D J, Cottam M G and Legrand S 1981 *J. Phys. C: Solid State Phys.* **14** 945
[6] Lockwood D J, Mischler G, Zwick A, Johnstone I W, Psaltakis G C, Cottam M G, Legrand S and Léotin 1982 *J. Phys. C: Solid State Phys.* **15** 2973
[7] Vianna S S, de Araújo C B and Rezende S 1984 *Phys. Rev.* B **30** 3516
[8] Lockwood D J and Cottam M G 1988 *J. Appl. Phys.* **64** 5876
[9] Belanger D P, King A R, Jaccarino V and Cardy J L 1983 *Phys. Rev.* B **28** 2522
Ferreira I B, Cardy J L, King A R and Jaccarino V 1991 *Phys. Rev.* B at press
[10] Kleemann W and Uhlig R 1989 *J. Phys.: Condens. Matter* **1** 1653
[11] Baltensperger W and Helman J S 1968 *Helv. Phys. Acta* **41** 668
[12] Elliott R J, Krumhansl J A and Leath P L 1974 *Rev. Mod. Phys.* **46** 465
[13] Schäfer F J and Kleemann W 1985 *J. Appl. Phys.* **57** 2606
[14] Striefler M E and Barsch G R 1973 *Phys. Status Solidi* b **59** 205
[15] Stanley H E 1971 *Introduction to Phase Transitions and Critical Phenomena* (Oxford: Oxford University Press) p 90
[16] Ziman J M 1963 *Electrons and Phonons* (Oxford: Oxford University Press) p 154
[17] Touloukian Y S and Buyco E H 1970 *Thermodynamical Properties of Matter* vol 5 *Specific Heat of Nonmetallic Solids* (New York: Plenum) p 940; 1027
[18] Jahn I R 1973 *Phys. Status Solidi* b **57** 681
[19] Cerdeira F, Fjeldly T A and Cardona M 1973 *Phys. Rev.* B **8** 4734
[20] Bechstedt F and Peuker K 1975 *Phys. Status Solidi* b **72** 743
[21] Silvera I F and Tinkham M 1964 *Bull. Am. Phys. Soc.* **9** 714
[22] Katiyar R S 1970 *J. Phys. C: Solid State Phys.* **3** 1087
[23] Katiyar R S 1970 *J. Phys. C: Solid State Phys.* **3** 1693